Report

Current Biology

DOF2.1 Controls Cytokinin-Dependent Vascular Cell Proliferation Downstream of TMO5/LHW

Highlights

- DOF2.1 acts as a major transcriptional hub downstream of TMO5/LHW
- The CK-inducible DOF2.1 is sufficient to trigger periclinal and radial cell divisions
- DOF transcription factors redundantly regulate specific procambium divisions

Authors

Wouter Smet, Iris Sevilem, Maria Angels de Luis Balaguer, ..., Rosangela Sozzani, Ykä Helariutta, Bert De Rybel

Correspondence

yrjo.helariutta@slcu.cam.ac.uk (Y.H.), beryb@psb.vib-ugent.be (B.D.R.)

In Brief

Smet et al. capture the transcriptional responses upon simultaneous TMO5/LHW induction and identify DOF2.1 as part of the cytokinin-dependent downstream responses. Furthermore, they show that DOF2.1 and its closest homologs control periclinal and radial procambium divisions in distinct zones of this tissue.

Smet et al., 2019, Current Biology 29, 520–529
February 4, 2019
https://doi.org/10.1016/j.cub.2018.12.041

CellPress

CellPress

Current Biology
Report

DOF2.1 Controls Cytokinin-Dependent Vascular Cell Proliferation Downstream of TMO5/LHW

Wouter Smet,[1,2,3,10] Iris Sevilem,[4,5,10] Maria Angels de Luis Balaguer,[6] Brecht Wybouw,[1,2] Eliana Mor,[1,2] Shunsuke Miyashima,[4,7] Bernhard Blob,[9] Pawel Roszak,[4,9] Thomas B. Jacobs,[1,2] Mark Boekschoten,[8] Guido Hooiveld,[8] Rosangela Sozzani,[6] Ykä Helariutta,[4,5,9,*] and Bert De Rybel[1,2,3,11,*]

[1]Ghent University, Department of Plant Biotechnology and Bioinformatics, Technologiepark 71, 9052 Ghent, Belgium
[2]VIB Center for Plant Systems Biology, Technologiepark 71, 9052 Ghent, Belgium
[3]Wageningen University, Laboratory of Biochemistry, Stippeneng 4, 6708 WE Wageningen, the Netherlands
[4]Institute of Biotechnology, HiLIFE, University of Helsinki, Viikinkaari 5d, 00014 Helsinki, Finland
[5]Organismal and Evolutionary Biology Research Programme, Faculty of Biological and Environmental Sciences, University of Helsinki, 00014 Helsinki, Finland
[6]Department of Plant and Microbial Biology, North Carolina State University, Raleigh, NC 27695, USA
[7]Graduate School of Sciences and Technology, Nara Institute of Science and Technology, Nara, 630-0192 Japan
[8]Wageningen University, Division of Human Nutrition and Health, Nutrition, Metabolism and Genomics group, Stippeneng 4, 6708 WE Wageningen, the Netherlands
[9]Sainsbury Laboratory, University of Cambridge, Bateman Street, Cambridge CB2 1LR, UK
[10]These authors contributed equally
[11]Lead Contact
*Correspondence: yrjo.helariutta@slcu.cam.ac.uk (Y.H.), beryb@psb.vib-ugent.be (B.D.R.)
https://doi.org/10.1016/j.cub.2018.12.041

SUMMARY

To create a three-dimensional structure, plants rely on oriented cell divisions and cell elongation. Oriented cell divisions are specifically important in procambium cells of the root to establish the different vascular cell types [1, 2]. These divisions are in part controlled by the auxin-controlled TARGET OF MONOPTEROS5 (TMO5) and LONESOME HIGHWAY (LHW) transcription factor complex [3–7]. Loss-of-function of *tmo5* or *lhw* clade members results in strongly reduced vascular cell file numbers, whereas ectopic expression of both TMO5 and LHW can ubiquitously induce periclinal and radial cell divisions in all cell types of the root meristem. TMO5 and LHW interact only in young xylem cells, where they promote expression of two direct target genes involved in the final step of cytokinin (CK) biosynthesis, *LONELY GUY3* (*LOG3*) and *LOG4* [8, 9] Therefore, CK was hypothesized to act as a mobile signal from the xylem to trigger divisions in the neighboring procambium cells [3, 6]. To unravel how TMO5/LHW-dependent cytokinin regulates cell proliferation, we analyzed the transcriptional responses upon simultaneous induction of both transcription factors. Using inferred network analysis, we identified *AT2G28510/DOF2.1* as a cytokinin-dependent downstream target gene. We further showed that DOF2.1 controls specific procambium cell divisions without inducing other cytokinin-dependent effects such as the inhibition of vascular differentiation. In summary, our results suggest that *DOF2.1* and its closest homologs control vascular cell proliferation, thus leading to radial expansion of the root.

RESULTS

Simultaneous Induction of *TMO5/LHW* Results in Cell Proliferation

To dissect the transcriptional responses downstream of TMO5/LHW, we generated a double dexamethasone (DEX)-inducible line by fusing TMO5 and LHW to the glucocorticoid receptor (GR) tag and driving them from the strong meristematic *RPS5A* promoter [10]. As expected, the number of cell files (quantified as total number of cell files in radial sections halfway between the quiescent center and the elongation zone) in the root apical meristem was strongly increased in the p*RPS5A*::*TMO5*:GR x p*RPS5A*::*LHW*:GR (henceforth named double-GR or dGR) line compared to the control line upon a 24 h induction (Figures 1A–1D). In our experimental conditions, the dGR line resulted in much stronger induction of periclinal and radial divisions (PRD, Figure S1A) compared to the single TMO5-GR or LHW-GR lines (Figures S1B and S1C). Although the constitutive TMO5/LHW misexpression line [4] resulted in significantly more divisions, the dGR line showed a very predictable increase in the number of cell divisions (Figures S1B and S1C). Intriguingly, the first PRD already occurred after 4 h of DEX induction in the dGR line (Figures 1E–1H), while these divisions were not observed in control plants. These results suggest that all transcriptional changes required for PRD already occurred before this time. Also, prolonged induction of the dGR line resulted in cumulatively more PRD (Figures 1I and S1D).

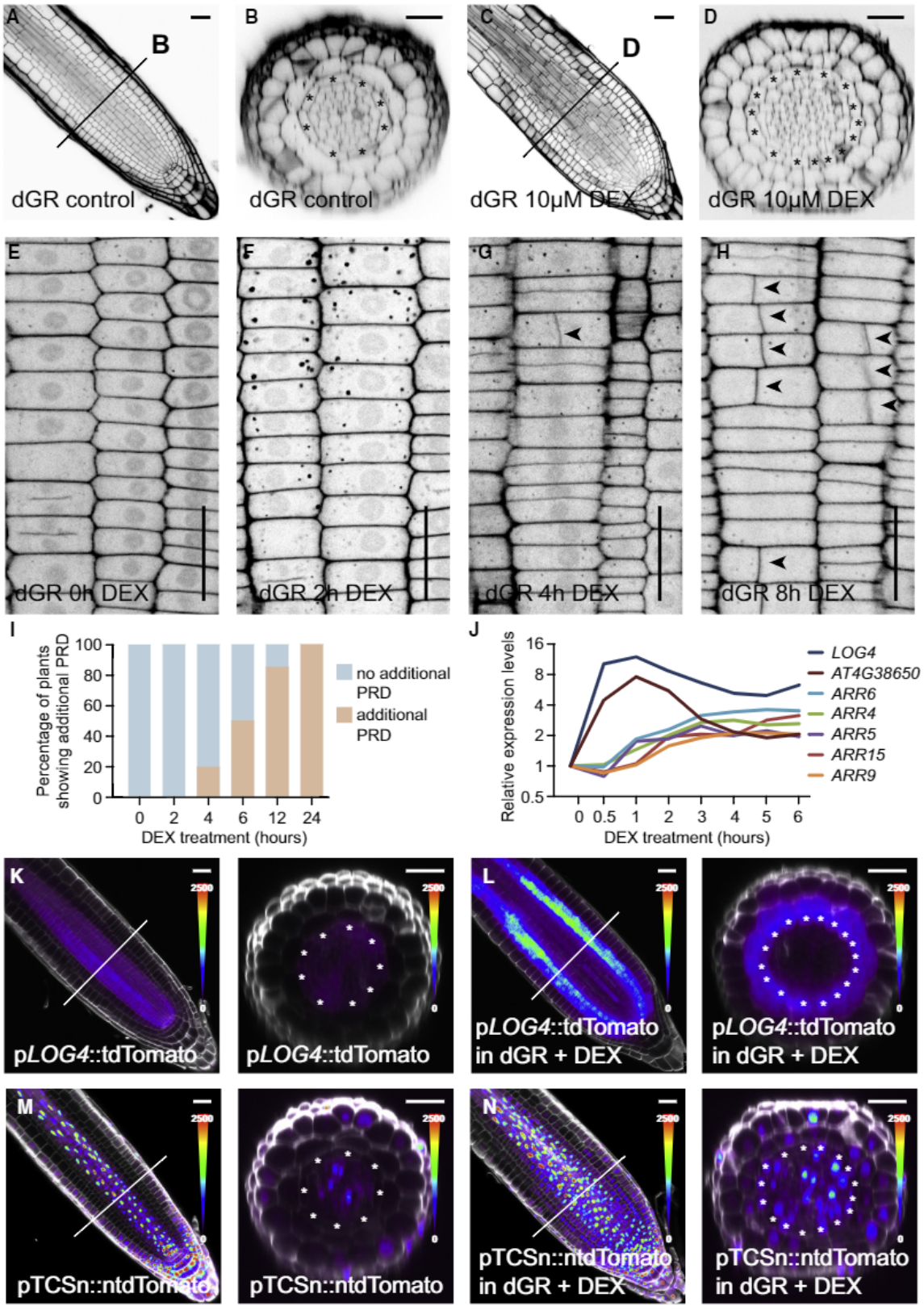

(legend on next page)

Identification of DOF2.1 as Transcriptional Hub Downstream of TMO5/LHW

We next interrogated the genome-wide transcriptional responses upon TMO5/LHW induction in a high-density time course experiment. After statistical analysis (fold change > 2, q value < 0.05, see STAR Methods for details), 237 genes were identified as significantly upregulated at one or more of the time points (Table S1). We confirmed the regulation of a selection of 25 genes by qRT-PCR analysis, which included known TMO5/LHW target genes (Table S2). In line with previous data [3, 6, 11, 12], the cytokinin (CK) biosynthesis genes, *LOG3* and *LOG4*, and other known targets, *SACL3* and *AT4G38650*, were quickly and strongly upregulated (Figure 1J and Table S2). Intriguingly, following this first wave of direct target responses at 0.5–1 h of induction, a second wave of gene expression including A-type *ARABIDOPSIS RESPONSE REGULATORS* (*ARRs*) [13, 14] was observed between 1–3 h of DEX treatment (Figure 1J and Table S2). Given that CK biosynthesis through *LOG3* and *LOG4* genes is activated at the 0.5–1 h time point, induction of downstream CK signaling reported by A-type *ARR* genes was expected, but not reported so far. Next, to understand the spatial aspects of dGR induction, reporters for CK biosynthesis (p*LOG4*::tdTomato) and CK signaling (pTCSn::ntdTomato) were analyzed. *LOG4* is expressed along the xylem axis and in protoxylem associated pericycle and endodermis, whereas TCSn is expressed in procambium, columella, epidermis, and root cap cells (Figures 1K and 1M). Upon induction, *LOG4* and TCSn were ectopically expressed outside of their normal domain in the root meristem (Figures 1L and 1N), confirming the activation of CK biosynthesis and CK signaling in all cell types in the root meristem upon induction of dGR.

As our high-resolution time-course dataset allowed the identification of consecutive waves of gene expression upon *TMO5/LHW* induction, we wanted to identify downstream transcriptional hubs using network inference analysis [15]. To infer relationships and relative importance in the differentially expressed genes, we utilized the GENIST regulatory network inference algorithm [15]. The application of GENIST resulted in 6 individual networks, corresponding to pairwise comparisons between the 0 h and all consecutive time points of the TMO5/LHW induction time course in which 0.5 h and 1 h were combined into one set (0 –0.5+1 h, 0–2h, 0–3 h, 0–4 h, 0–5 h, and 0–6 h) (see STAR Methods for details). Both *TMO5* and *LHW* were included in the network to provide a starting point for the transcriptional cascade. To illustrate the cascade of regulations through time, the networks were color coded for each time point (Figure S2, see Data S2 for more information). A first wave of gene expression (red), starting from *TMO5*, includes its direct target genes. This is followed by a second wave (green), including CK response marked by *ARRs*. A third wave of gene expression (blue) includes several major nodes each controlling a high number of genes and thus marking the point where a large transcriptional change occurs. Notably, one of the most prominent nodes corresponded to *AT2G28510/DOF2.1*; a DOF-type TF previously suggested to be expressed in vascular tissues [16, 17]. To investigate this regulatory network in more detail and highlight significant regulations, we generated a subnetwork focusing only on *TMO5*, *ARR12*, *DOF2.1*, and their predicted direct target genes (see Data S2 for more information). First, this network correctly predicts *TMO5* to regulate all known target genes, including *SACL3* (represented as *uORF34* and *uORF35*), *BUD2*, *LOG3*, and *LOG4*, thus confirming earlier results [3, 6, 11, 12]. Second, *DOF2.1* is predicted to act downstream of *ARR12*, not *TMO5*, suggesting that this gene might not be a direct target gene but is likely regulated by CK signaling pathway, which is reported to be activated by TMO5/LHW (see Data S2 for more information).

DOF2.1 Expression Is Controlled by TMO5/LHW-Dependent CK

To investigate the role of *DOF2.1* as a downstream target of TMO5/LHW, we first generated a transcriptional p*DOF2.1*::GUS-GFP reporter line. During embryogenesis, *DOF2.1* is first expressed in the upper tier in heart stage (Figures 2A–2C) and shows expression in the embryonic root at torpedo stage (Figure 2C). Post-embryonically, *DOF2.1* shows weak expression in the aerial tissues and high expression throughout the root (Figures S3A and S3B). Specifically, in the root apical meristem, *DOF2.1* is strongly expressed in xylem pole pericycle cells, in specific neighboring procambium cells, and in the flanking endodermal cells (Figures 2D and 2E), suggesting that the bilateral symmetry of the root might extend beyond the central vascular cylinder [18]. Given that some DOF-type TFs have been reported to be mobile [19], we next investigated if the 31.8 kDa DOF2.1 protein might be a mobile factor. Protein accumulation of a translational p*DOF2.1*::*DOF2.1*:YFP fusion recapitulated the expression pattern of the transcriptional reporter line (Figures 2F and 2G), suggesting that DOF2.1 is not moving outside of its domain of expression. We next examined *DOF2.1* expression upon TMO5/LHW induction and observed that *DOF2.1* expression extended outside its normal domain and into the ground tissue cells neighboring the phloem poles (Figures 2H and 2I). Notably, no expression of *DOF2.1*, both prior and upon induction of TMO5/LHW, was observed in xylem, centrally located procambium or the phloem lineage cells. However, the *RPS5A* promoter is expressed in this zone (Figure 2J), and CK signaling

Figure 1. Simultaneous Induction of TMO5/LHW Results in Cell Proliferation

(A–D) Confocal sections of untreated (A-B) and induced (C-D) dGR root meristems. Lines in A and C represent radial cross-sections of B and D, respectively.

(E–H) Longitudinal optical sections of cortical cells in dGR root meristems treated with 10μM dexamethasone (DEX) for the indicated amount of time. Arrowheads mark induced PRD

(I) Percentage of dGR plants showing additional periclinal and/or radial cell divisions (PRD) in time. Plants were scored to have additional PRD if one or more of these divisions were observed ectopically in longitudinal confocal sections.

(J) Relative expression levels of genes in transcriptome data upon induction of the dGR line.

(K–N) Expression of p*LOG4*::tandemTomato and pTCSn::ntandemTomato in dGR after mock treatment and after 24h DEX treatment. Asterisks indicate endodermis.

Scale bars in (A)–(H) and (K)–(N): 25μm. See also Figures S1 and S2, Tables S1 and S2, and Data S1 and S2.

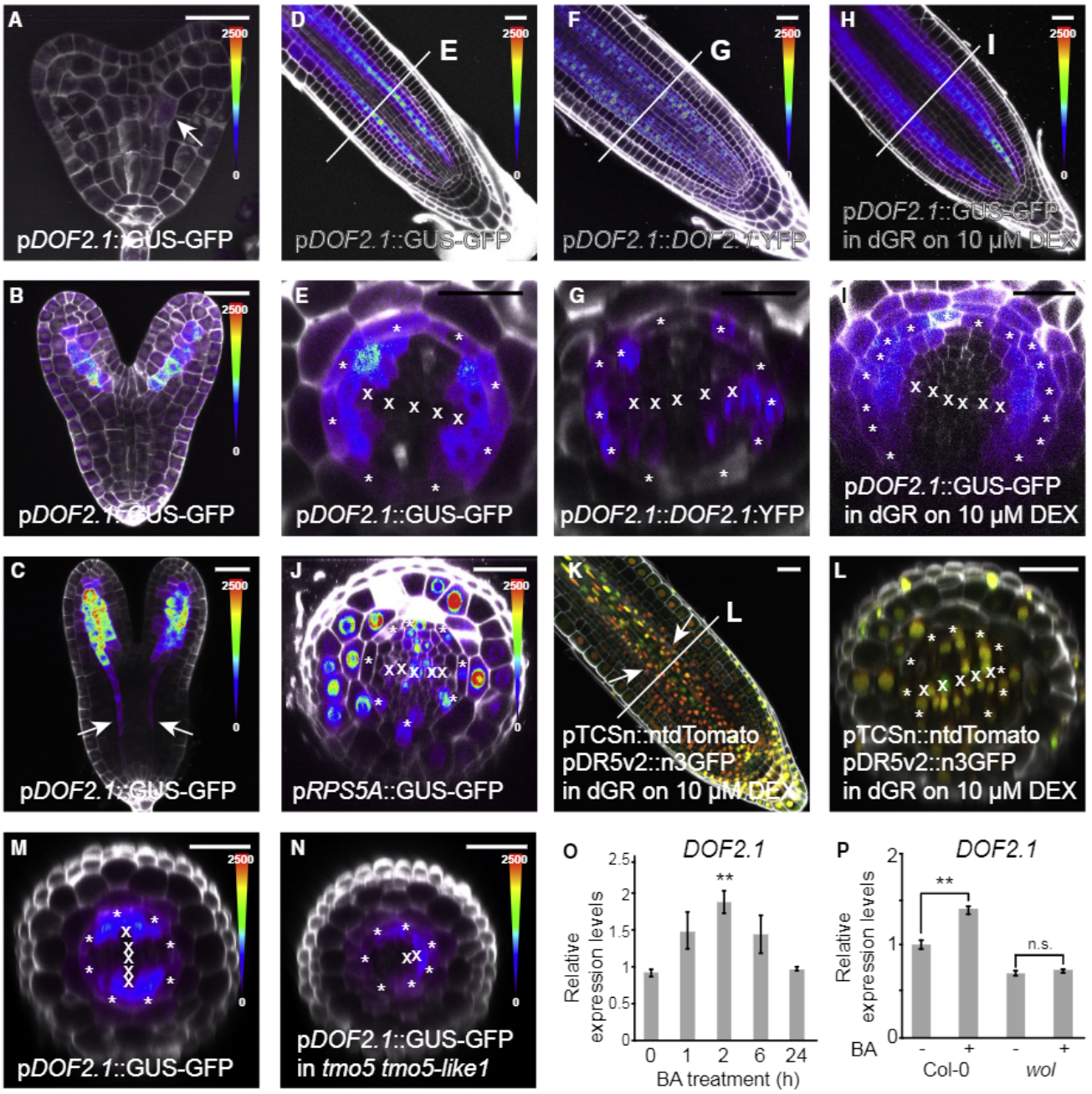

Figure 2. DOF2.1 Expression in Xylem-Pole-Associated Cells

(A–C) Expression of p*DOF2.1*::GFP-GUS during embryogenesis. Arrows indicate expression in the embryonic root.

(D–I) Optical sections of the primary root meristems of p*DOF2.1*::GUS-GFP (D and E), p*DOF2.1::DOF2.1*:YFP (F and G) and p*DOF2.1*::GFP-GUS in dGR upon 24h DEX treatment (H and I).

(J) Optical cross section of p*RPS5A*::nGFP-GUS in the root meristem.

(K and L) TCSn::ntdTomato-DR5revV2::n3GFP expression in dGR after 24h DEX treatment. The line in (K) represents the optical cross section shown in (L).

(M and N) p*DOF2.1*::GUS-GFP expression in Col-0 and *tmo5 tmo5like1* double mutant background.

(O) Relative expression levels of *DOF2.1* upon treatment with 10 μM Benzyl Adenine (BA) for 0, 1, 2, 6, and 24 h as determined by qRT-PCR analysis.

(P) Relative expression levels of *DOF2.1* upon treatment with 10 μM BA in Col-0 and *wol* mutant backgrounds.

In all qRT-PCR experiments, data are represented as mean ± SEM and asterisks indicate significance (**$p < 0.001$; n.s.: not significant) as determined by two-sided t-tests. In all confocal images, asterisks indicate endodermis and crosses indicate xylem cells; scale bars, 25 μm. See also Figures S1, S2, S3 and Data S1.

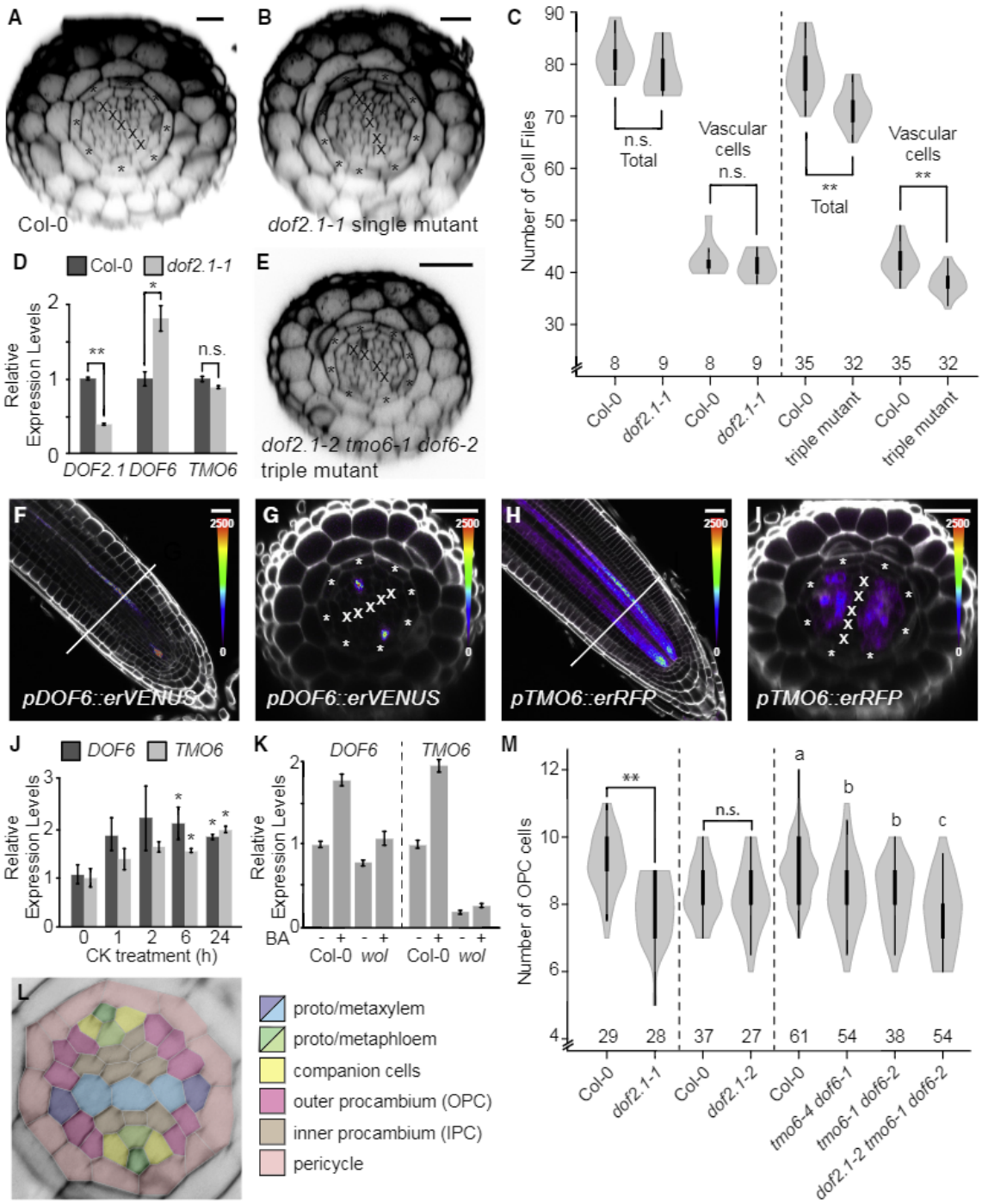

Figure 3. DOF2.1 Controls Specific Procambium Divisions

(A, B, and E) Optical sections of root meristems of Col-0, *dof2*.1-1 and *dof2.1-2 tmo6-1 dof6-2*, respectively.

(C) Quantification of the cell file number of *dof2.1* (left panel) and *dof2.1-2 tmo6-1 dof6-2* (triple mutant) (right panel) with respective controls.

(D) Relative expression levels of *DOF2.1*, *DOF6* and *TMO6* in Col-0 and *dof2.1-1* as determined by qRT-PCR analysis.

(F–I) p*DOF6*::erVENUS and p*TMO6*::erRFP expression in root apical meristems. Location of cross sections in G and I are indicates with lines in F and H respectively.

(J) Relative expression levels of *DOF6* and *TMO6* upon treatment with 10 μM BA for 0, 1, 2, 6 and 24h as determined by qRT-PCR analysis.

(K) Relative expression levels of *DOF6* and *TMO6* upon 2 h treatment with 10 μM BA in Col-0 and *wol* mutant backgrounds.

(L) Schematic overview of different cell types in the vascular bundle, indicating OPC and IPC cells.

(M) Quantification of OPC cell numbers in the mutant backgrounds indicated with the respective controls.

(legend continued on next page)

(but not auxin signaling) is activated in these cells by TMO5/LHW [3, 6] as visualized by a newly generated dual color, single locus auxin/CK-signaling reporter line (pTCSn::ntdTomato - pDR5revV2::n3GFP) (Figures 2K and 2L). These results suggest an active suppression of *DOF2.1* expression in the center of the root vasculature. To provide additional evidence that *DOF2.1* acts downstream of TMO5/LHW, we first analyzed its relative expression levels in *lhw* single and *tmo5 tmo5-like1* double mutant backgrounds by qRT-PCR and found that these were reduced (Figure S3F). Because these mutants have a reduced vascular bundle with only one xylem pole and *DOF2.1* is mostly expressed in this area, it could well be that the observed result is due to the altered anatomy of these mutants. Hence, we introduced the p*DOF2.1*::GUS-GFP reporter line in the *tmo5 tmo5-like1* double mutant background to observe changes in the tissue specific expression levels. Expression level was reduced in this mutant backgrounds supporting that *DOF2.1* expression depends on functional TMO5/LHW (Figures 2M and 2N).

Next, given that *DOF2.1* is induced later than *LOG4* upon TMO5/LHW induction (3-4h for *DOF2.1* compared to 0.5-1h for *LOG4*, see Table S1-**2**); that the *DOF2.1* expression pattern is very similar to that of *LOG3* and *LOG4* [3] and that our network analysis predicts *DOF2.1* to act downstream of ARR12 (Table S2), we questioned if *DOF2.1* could act downstream of the TMO5/LHW-dependent CK biosynthesis. Indeed, *DOF2.1* transcript levels were quickly induced in root meristems by exogenous CK treatments in a qRT-PCR experiment (Figure 2O) and in seedlings [20, 21]; but this induction was abolished in a *wooden leg* (*wol*) mutant background (Figure 2P). These results suggest that *DOF2.1* is transcriptionally controlled by CK. A CK-dependent regulation of *DOF2.1* expression levels was further supported by several recent reports showing direct binding of the well-known B-type ARRs executors of CK signaling ARR1, ARR10, and ARR12 to the *DOF2.1* promoter region [21, 22]. Thus, although we cannot exclude additional CK-independent regulation of *DOF2.1* at the moment, collectively, these results suggest that *DOF2.1* acts downstream of the TMO5/LHW-dependent CK biosynthesis.

DOF2.1 and Its Close Homologs Control Vascular Cell Proliferation

As the inferred network analysis predicts that *DOF2.1* would act as a major downstream transcriptional hub, we next questioned whether this CK-inducible DOF-type TF is indeed involved in controlling vascular cell proliferation. Given that a single *dof2.1* loss-of-function did not result in obvious phenotypes (Figures 3A–3C) and the possible redundancy in the large DOF-type TF family, we quantified the relative expression levels of the two closest homologs, namely *TMO6* and *DOF6* (Figure S3E), in the *dof2.1* line. The relative expression levels of the latter were upregulated (Figure 3D), hinting toward compensatory regulation. Hence, we generated a triple mutant of *DOF2.1*, *DOF6*, and *TMO6* to overcome the redundancy within this subclade of the DOF transcription factor family using the CRISPR/Cas9 system (Figure S4). Using confocal cross sections to quantify the number of cell files in the root meristem, the *dof2.1-2 tmo6-1 dof6-2* triple mutant showed a significant reduction in the total number of cell files and in the number of vascular cell files when compared to Col-0 (Figures 3C and 3E), suggesting that these closely related DOF-type TFs act in a redundant manner to control vascular proliferation. To further examine the redundancy of these factors, we analyzed the expression patterns of p*TMO6* and p*DOF6* and found that they are only partly overlapping but mostly distinct from the *DOF2.1* expression domain. *DOF6* shows sieve element specific expression, and the *TMO6* reporter line is more broadly expressed in phloem-associated procambium cells (Figures 3F–3I). Intriguingly, *TMO6* and *DOF6* are also CK inducible (Figure 3J) in a wild-type, but not a *wol*, background (Figure 3K) and are mildly regulated in the transcriptome data-set (Figure S3J). To investigate the potential that these factors regulate specific divisions in the procambium based on their expression domains, we quantified the number of procambium cells in single-, double-, and triple-mutant combinations using optical cross sections. Additionally, we quantified both procambium cells associated with the protoxylem pole next to the pericycle (where DOF2.1 is mostly expressed: outer procambium cells - OPC) as well as those associated with the phloem pole toward the inside of the vascular bundle (showing no *DOF2.1* expression: inner procambium cells - IPC) (Figure 3L). The number of OPC cell files was significantly reduced in *dof2.1-1* (Figure 3M). Although a second *dof2.1-2* allele did not show a reduction by itself, it did significantly enhance the effect of the *tmo6-1 dof6-2* double mutant, suggesting that both alleles are functional. On the contrary, neither of the *dof2.1* alleles had a significant effect on the number of IPC cells (Figure S3J), while multiple *dof6 tmo6* double mutant combinations significantly reduced IPC numbers (Figure S3J). Thus, these results suggest that DOF2.1 specifically controls the number of OPC divisions, while TMO6 and DOF6 show the strongest effect toward the IPC cell numbers. Intriguingly, the *dof2.1-2 tmo6-1 dof6-2* triple mutant also showed a mild reduction in the number of vascular cell files in mature embryos (Figure S3H), suggesting that these DOF-type TF might act from embryogenesis onward. Taken together, multiple DOF-type TFs control cell divisions in specific sets of procambium cells during early vascular development.

Next, to investigate whether DOF2.1 is sufficient to induce PRD, we generated an inducible p*RPS5A*::*DOF2.1*:*GR* misexpression line. Upon induction, this line showed an increased number of cell files for each cell type in the root meristem when compared to Col-0 (Figures 4A–4D). To gain insights into the temporal dynamics, we next analyzed this induction of PRD in a time series experiment. Similar to what we observed after TMO5/LHW induction (Figures 1E–1H), p*RPS5A*::*DOF2.1*:*GR* showed the first radial divisions after only 6 h DEX induction

In all qRT-PCR experiments and cell number quantifications, data are represented as mean ± SEM and asterisks indicate significance (**$p < 0.001$; *$p < 0.05$; n.s.: not significant) as determined by two-sided t-tests; small case letters in M indicate significantly different groups as determined using a one-way ANOVA with post hoc Tukey HSD testing and sample numbers are indicated above the x axis. In all confocal images, asterisks indicate endodermis and crosses indicate xylem cells; scale bars, 25 μm. See also Figure S3 and S4 and Data S1.

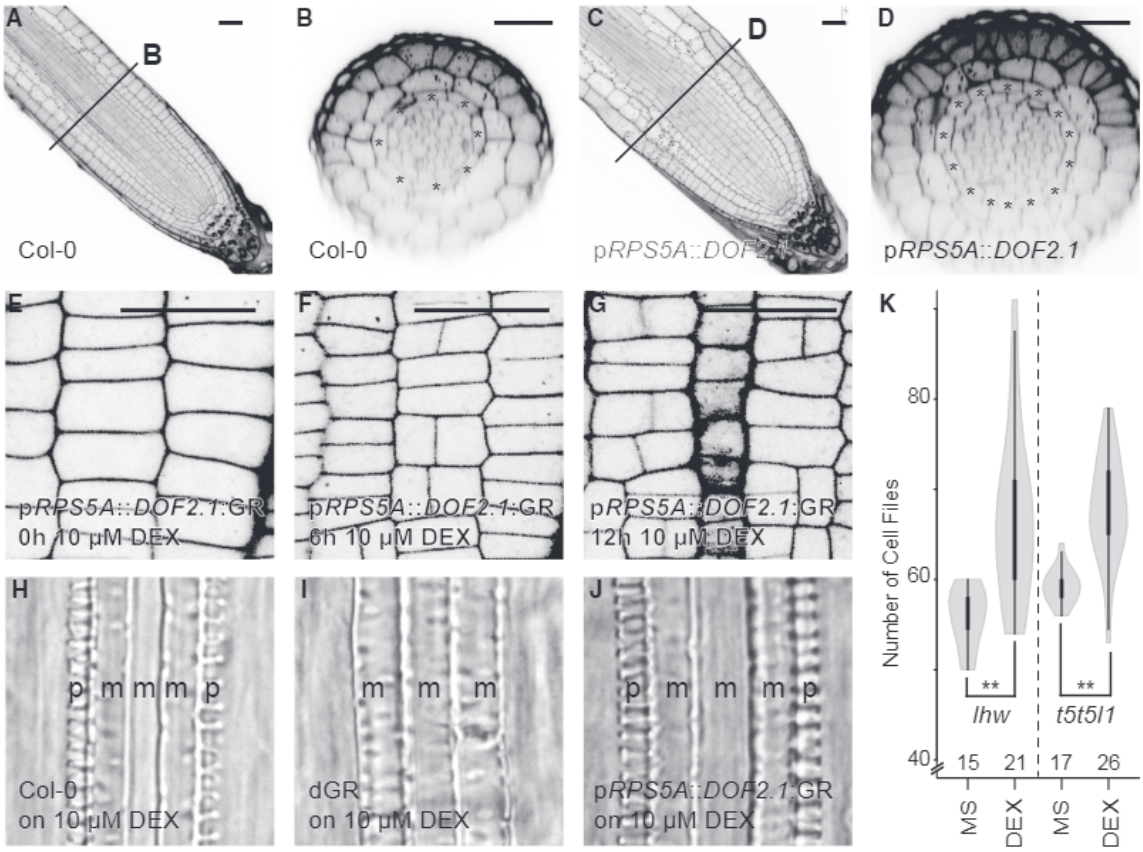

Figure 4. DOF2.1 Is Sufficient to Trigger PRD

(A–D) Optical sections of Col-0 and p*RPS5A*::DOF2.1. Lines in A and C indicate position of cross sections in B and D respectively.

(E–G) Longitudinal sections of the epidermis in p*RPS5A*::*DOF2.1*:GR after DEX induction for the indicated time.

(H–J) DIC images of the differentiated vasculature of Col-0, dGR and p*RPS5A*::*DOF2.1*:GR in five-day-old seedlings.

(K) Quantification of the cell file number in *lhw* and *tmo5 tmo5like1* mutant backgrounds harboring the p*RPS5A*::*DOF2.1*:GR rescue construct with (DEX) and without (MS) treatment with 10μM DEX.

In all cell number quantifications, asterisks indicate significance (**$p < 0.001$) as determined by two-sided t-tests and sample numbers are indicated above the x axis. In all confocal images, asterisks indicate endodermis; scale bars, (A)–(D) 25 μm, (E)–(G) 10 μm. See also Figure S3 and Data S1.

(Figures 4E–4G and S3I). Although a similar effect was observed upon inducing *TMO5/LHW* or *DOF2.1*, the former involves the activation of CK biosynthesis. As such, the effects of constitutive TMO5/LHW overexpression are not limited to induction of PRD but also include other CK-related phenotypes such as inhibition of protoxylem cell differentiation [3, 6]. Following the logic that DOF2.1 acts downstream of CK signaling, plants with elevated *DOF2.1* levels exhibit normally differentiated protoxylem cells (Figures 4H–4J), suggesting that DOF2.1 specifically controls vascular proliferation without causing other pleiotropic CK-related effects. Nevertheless, likely due to divisions of the young xylem cells, constitutive misexpression of *DOF2.1* occasionally showed the formation of additional protoxylem cell files with normal differentiation (Figures S3C and S3D). Next, we introduced the p*RPS5A*::*DOF2.1*:GR line into the *tmo5 tmo5-like1* double and *lhw* single mutants [4, 23]. Induction of *DOF2.1* led to an increase in the total number of cell files of the root meristem in both *tmo5 tmo5-like1* double and *lhw* single mutant backgrounds (Figure 4K). Thus, these results suggest that DOF2.1 acts as a transcriptional hub downstream of TMO5/LHW and is both required and sufficient to controlling vascular cell proliferation.

DISCUSSION

Although over 200 genes were identified as being transcriptionally upregulated upon simultaneous induction of TMO5 and LHW, only a few were suggested to act as major transcriptional hubs in the inferred network analysis. We focused our attention to one of these, *DOF2.1*, previously reported to be expressed in vascular tissues [17]. We showed that *DOF2.1* acts downstream of the TMO5/LHW-dependent cytokinin response and, together with its closest homologs, controls vascular proliferation. Several other DOF-type transcription factors have been reported to be expressed in vascular tissues [17, 19], suggesting a more prominent role for this family of transcription factors in regulating vascular development. For example, DOF5.6/HCA2 was reported to be involved in controlling divisions in the interfascicular cambium although no phenotypes were observed in root tissues [24]. Given that the observed reduction in cell file

number is weaker in the triple *dof2.1-2 tmo6-1 dof6-2* mutant compared to the reduction observed in higher order mutants of the *tmo5* of *lhw* subclades [4], it is likely that more DOF family members are involved in controlling this process. However, *DOF2.1* is the only DOF-type transcription factor we clearly identified as TMO5/LHW target, suggesting that other members of this large transcription factor family are likely to be under control of different signals or might act during different stages of development.

Here, we showed that at least three DOF-type transcription factors DOF2.1, TMO6, and DOF6 control specific subsets of procambium cell divisions leading to vascular proliferation in the root meristem, with DOF2.1 specifically controlling OPC divisions, while TMO6 and DOF6 have the strongest effect on IPC cell numbers. This differential response suggests that the procambium is not a homogeneous pool of cells. Indeed, distinct zones might exist along the longitudinal and radial axis of procambial tissue, showing differential properties in cell division potential and thus also regulatory mechanisms. In this aspect, it would be interesting to investigate the contribution of these cell populations to secondary growth when procambium cells are reactivated.

DOF2.1 is specifically expressed in cells surrounding the xylem poles but remains absent from the central region of the vascular bundle even when ectopically expressed in this domain. This observation suggests that *DOF2.1* expression levels might be actively repressed in this zone. Intriguingly, CLASS III HOMEODOMAIN LEUCINE ZIPPER (HD-ZIPIII) transcription factors are expressed in this central region and have been shown to act as negative regulators of cell proliferation [25]. Besides the fact that several DOF factors have been identified as binding to the promoter regions of HD-ZIPIII genes [26], it would be interesting to investigate if these factors might at the same time act as negative regulators of DOF-type TF expression.

STAR★METHODS

Detailed methods are provided in the online version of this paper and include the following:

- KEY RESOURCES TABLE
- CONTACT FOR REAGENT AND RESOURCE SHARING
- EXPERIMENTAL MODEL AND SUBJECT DETAILS
- METHOD DETAILS
  - Plant material and growth conditions
  - Cloning and plant transformation
  - CRISPR/CAS9 mutant generation
  - Plant imaging and image processing
  - qRT-PCR
  - Whole genome transcriptome analysis
  - Network inference
- QUANTIFICATION AND STATISTICAL ANALYSIS
- DATA AND SOFTWARE AVAILABILITY

SUPPLEMENTAL INFORMATION

Supplemental Information includes four figures, two tables, and two data files and can be found with this article online at https://doi.org/10.1016/j.cub.2018.12.041.

ACKNOWLEDGMENTS

The authors acknowledge Jenny Jansen for technical assistance with microarray hybridizations and Dolf Weijers for helpful discussions and suggestions. W.S. was funded by the Netherlands Organization for Scientific Research (NWO; VIDI-864.13.001). B.W. and B.D.R. were funded by The Research Foundation - Flanders (FWO; Odysseus II G0D0515N and Post-doc grant 12D1815N, respectively). E.M. was funded on a European Research Council grant (ERC; StG TORPEDO; 714055). Y.H. was funded by Finnish Centre of Excellence in Molecular Biology of Primary Producers (Academy of Finland CoE program 2014-2019) decision #271832, the Gatsby Foundation [GAT3395/PR3]), University of Helsinki (award 799992091) and the European Research Council Advanced Investigator Grant SYMDEV [No. 323052]. S.M. was funded by a JSPS postdoctoral fellowship for research abroad. Support to R.S. was provided by the National Science Foundation (NSF) (CAREER MCB 1453130) and bilaterally by the NSF and the Biotechnology and Biological Sciences Research Council (BBSRC) (NSF MCB-1517058) to R.S. and Y.H.

AUTHOR CONTRIBUTIONS

B.D.R. and Y.H. conceived the project; W.S. and B.D.R. designed experiments; W.S., I.S., B.W., E.M, P.W. and S.M. performed most of the experiments; T.B.J. assisted setting up the CRISPR/Cas9 system; B.B. assisted in generated mutant alleles; M.A.d.L.B. and R.S. performed the network inference analysis; M.B. and G.H. processed and analyzed the transcriptome data; B.D.R. supervised the project; W.S. and B.D.R. wrote the paper with input from all authors.

DECLARATION OF INTERESTS

Part of this work is included in a patent filing: GB 1817464.9; MEANS AND METHODS TO INCREASE ORGAN SIZE IN PLANTS.

Received: July 27, 2018
Revised: November 12, 2018
Accepted: December 21, 2018
Published: January 24, 2019

REFERENCES

1. Dolan, L., Janmaat, K., Willemsen, V., Linstead, P., Poethig, S., Roberts, K., and Scheres, B. (1993). Cellular organisation of the Arabidopsis thaliana root. Development *119*, 71–84.
2. Jürgens, G.M.U. (1994). Arabidopsis. In Embryos: Colour Atlas of Development - Bard,Jbl. Nature *370*, 190–190.
3. De Rybel, B., Adibi, M., Breda, A.S., Wendrich, J.R., Smit, M.E., Novák, O., Yamaguchi, N., Yoshida, S., Van Isterdael, G., Palovaara, J., et al. (2014). Plant development. Integration of growth and patterning during vascular tissue formation in Arabidopsis. Science *345*, 1255215.
4. De Rybel, B., Möller, B., Yoshida, S., Grabowicz, I., Barbier de Reuille, P., Boeren, S., Smith, R.S., Borst, J.W., and Weijers, D. (2013). A bHLH complex controls embryonic vascular tissue establishment and indeterminate growth in Arabidopsis. Dev. Cell *24*, 426–437.
5. Ohashi-Ito, K., Matsukawa, M., and Fukuda, H. (2013). An atypical bHLH transcription factor regulates early xylem development downstream of auxin. Plant Cell Physiol. *54*, 398–405.
6. Ohashi-Ito, K., Saegusa, M., Iwamoto, K., Oda, Y., Katayama, H., Kojima, M., Sakakibara, H., and Fukuda, H. (2014). A bHLH complex activates vascular cell division via cytokinin action in root apical meristem. Curr. Biol. *24*, 2053–2058.
7. Ohashi-Ito, K., Oguchi, M., Kojima, M., Sakakibara, H., and Fukuda, H. (2013). Auxin-associated initiation of vascular cell differentiation by LONESOME HIGHWAY. Development *140*, 765–769.
8. Kuroha, T., Tokunaga, H., Kojima, M., Ueda, N., Ishida, T., Nagawa, S., Fukuda, H., Sugimoto, K., and Sakakibara, H. (2009). Functional

analyses of LONELY GUY cytokinin-activating enzymes reveal the importance of the direct activation pathway in Arabidopsis. Plant Cell *21*, 3152–3169.

9. Tokunaga, H., Kojima, M., Kuroha, T., Ishida, T., Sugimoto, K., Kiba, T., and Sakakibara, H. (2012). Arabidopsis lonely guy (LOG) multiple mutants reveal a central role of the LOG-dependent pathway in cytokinin activation. Plant J. *69*, 355–365.
10. Weijers, D., Franke-van Dijk, M., Vencken, R.J., Quint, A., Hooykaas, P., and Offringa, R. (2001). An Arabidopsis Minute-like phenotype caused by a semi-dominant mutation in a RIBOSOMAL PROTEIN S5 gene. Development *128*, 4289–4299.
11. Katayama, H., Iwamoto, K., Kariya, Y., Asakawa, T., Kan, T., Fukuda, H., and Ohashi-Ito, K. (2015). A Negative Feedback Loop Controlling bHLH Complexes Is Involved in Vascular Cell Division and Differentiation in the Root Apical Meristem. Curr. Biol. *25*, 3144–3150.
12. Vera-Sirera, F., De Rybel, B., Úrbez, C., Kouklas, E., Pesquera, M., Álvarez-Mahecha, J.C., Minguet, E.G., Tuominen, H., Carbonell, J., Borst, J.W., et al. (2015). A bHLH-based feedback loop restricts vascular cell proliferation in plants. Dev. Cell *35*, 432–443.
13. Kiba, T., Yamada, H., Sato, S., Kato, T., Tabata, S., Yamashino, T., and Mizuno, T. (2003). The type-A response regulator, ARR15, acts as a negative regulator in the cytokinin-mediated signal transduction in Arabidopsis thaliana. Plant Cell Physiol. *44*, 868–874.
14. To, J.P., Haberer, G., Ferreira, F.J., Deruère, J., Mason, M.G., Schaller, G.E., Alonso, J.M., Ecker, J.R., and Kieber, J.J. (2004). Type-A Arabidopsis response regulators are partially redundant negative regulators of cytokinin signaling. Plant Cell *16*, 658–671.
15. de Luis Balaguer, M.A., Fisher, A.P., Clark, N.M., Fernandez-Espinosa, M.G., Möller, B.K., Weijers, D., Lohmann, J.U., Williams, C., Lorenzo, O., and Sozzani, R. (2017). Predicting gene regulatory networks by combining spatial and temporal gene expression data in *Arabidopsis* root stem cells. Proc. Natl. Acad. Sci. USA *114*, E7632–E7640.
16. Yanagisawa, S. (2002). The Dof family of plant transcription factors. Trends Plant Sci. *7*, 555–560.
17. Gardiner, J., Sherr, I., and Scarpella, E. (2010). Expression of DOF genes identifies early stages of vascular development in Arabidopsis leaves. Int. J. Dev. Biol. *54*, 1389–1396.
18. Andersen, T.G., Naseer, S., Ursache, R., Wybouw, B., Smet, W., De Rybel, B., Vermeer, J.E.M., and Geldner, N. (2018). Diffusible repression of cytokinin signalling produces endodermal symmetry and passage cells. Nature *555*, 529–533.
19. Le Hir, R., and Bellini, C. (2013). The plant-specific dof transcription factors family: new players involved in vascular system development and functioning in Arabidopsis. Front. Plant Sci. *4*, 164.
20. Bhargava, A., Clabaugh, I., To, J.P., Maxwell, B.B., Chiang, Y.H., Schaller, G.E., Loraine, A., and Kieber, J.J. (2013). Identification of cytokinin-responsive genes using microarray meta-analysis and RNA-Seq in Arabidopsis. Plant Physiol. *162*, 272–294.
21. Zubo, Y.O., Blakley, I.C., Yamburenko, M.V., Worthen, J.M., Street, I.H., Franco-Zorrilla, J.M., Zhang, W., Hill, K., Raines, T., Solano, R., et al. (2017). Cytokinin induces genome-wide binding of the type-B response regulator ARR10 to regulate growth and development in *Arabidopsis*. Proc. Natl. Acad. Sci. USA *114*, E5995–E6004.
22. Xie, M.T., Chen, H.Y., Huang, L., O'Neil, R.C., Shokhirev, M.N., and Ecker, J.R. (2018). A B-ARR-mediated cytokinin transcriptional network directs hormone cross-regulation and shoot development. Nat. Commun. *9*, 1604.
23. Ohashi-Ito, K., and Bergmann, D.C. (2007). Regulation of the Arabidopsis root vascular initial population by LONESOME HIGHWAY. Development *134*, 2959–2968.
24. Guo, Y., Qin, G., Gu, H., and Qu, L.J. (2009). Dof5.6/HCA2, a Dof transcription factor gene, regulates interfascicular cambium formation and vascular tissue development in Arabidopsis. Plant Cell *21*, 3518–3534.
25. Carlsbecker, A., Lee, J.Y., Roberts, C.J., Dettmer, J., Lehesranta, S., Zhou, J., Lindgren, O., Moreno-Risueno, M.A., Vatén, A., Thitamadee, S., et al. (2010). Cell signalling by microRNA165/6 directs gene dose-dependent root cell fate. Nature *465*, 316–321.
26. Brady, S.M., Zhang, L., Megraw, M., Martinez, N.J., Jiang, E., Yi, C.S., Liu, W., Zeng, A., Taylor-Teeples, M., Kim, D., et al. (2011). A stele-enriched gene regulatory network in the Arabidopsis root. Mol. Syst. Biol. *7*, 459.
27. Kleinboelting, N., Huep, G., Kloetgen, A., Viehoever, P., and Weisshaar, B. (2012). GABI-Kat SimpleSearch: new features of the Arabidopsis thaliana T-DNA mutant database. Nucleic Acids Res. *40*, D1211–D1215.
28. Mähönen, A.P., Bonke, M., Kauppinen, L., Riikonen, M., Benfey, P.N., and Helariutta, Y. (2000). A novel two-component hybrid molecule regulates vascular morphogenesis of the Arabidopsis root. Genes Dev. *14*, 2938–2943.
29. Houbaert, A., Zhang, C., Tiwari, M., Wang, K., de Marcos Serrano, A., Savatin, D.V., Urs, M.J., Zhiponova, M.K., Gudesblat, G.E., Vanhoutte, I., et al. (2018). POLAR-guided signalling complex assembly and localization drive asymmetric cell division. Nature *563*, 574–578.
30. Liao, C.Y., Smet, W., Brunoud, G., Yoshida, S., Vernoux, T., and Weijers, D. (2015). Reporters for sensitive and quantitative measurement of auxin response. Nat. Methods *12*, 207–210, 2, 210.
31. Zürcher, E., Tavor-Deslex, D., Lituiev, D., Enkerli, K., Tarr, P.T., and Müller, B. (2013). A robust and sensitive synthetic sensor to monitor the transcriptional output of the cytokinin signaling network in planta. Plant Physiol. *161*, 1066–1075.
32. Lei, Y., Lu, L., Liu, H.Y., Li, S., Xing, F., and Chen, L.L. (2014). CRISPR-P: a web tool for synthetic single-guide RNA design of CRISPR-system in plants. Mol. Plant *7*, 1494–1496.
33. De Rybel, B., van den Berg, W., Lokerse, A., Liao, C.Y., van Mourik, H., Möller, B., Peris, C.L., and Weijers, D. (2011). A versatile set of ligation-independent cloning vectors for functional studies in plants. Plant Physiol. *156*, 1292–1299.
34. Wendrich, J.R., Liao, C.Y., van den Berg, W.A., De Rybel, B., and Weijers, D. (2015). Ligation-independent cloning for plant research. Methods Mol. Biol. *1284*, 421–431.
35. Brinkman, E.K., Chen, T., Amendola, M., and van Steensel, B. (2014). Easy quantitative assessment of genome editing by sequence trace decomposition. Nucleic Acids Res. *42*, e168.
36. Vanneste, S., De Rybel, B., Beemster, G.T.S., Ljung, K., De Smet, I., Van Isterdael, G., Naudts, M., Iida, R., Gruissem, W., Tasaka, M., et al. (2005). Cell cycle progression in the pericycle is not sufficient for SOLITARY ROOT/IAA14-mediated lateral root initiation in Arabidopsis thaliana. Plant Cell *17*, 3035–3050.
37. Truernit, E., Bauby, H., Dubreucq, B., Grandjean, O., Runions, J., Barthélémy, J., and Palauqui, J.C. (2008). High-resolution whole-mount imaging of three-dimensional tissue organization and gene expression enables the study of Phloem development and structure in Arabidopsis. Plant Cell *20*, 1494–1503.
38. Kurihara, D., Mizuta, Y., Sato, Y., and Higashiyama, T. (2015). ClearSee: a rapid optical clearing reagent for whole-plant fluorescence imaging. Development *142*, 4168–4179.
39. Ursache, R., Andersen, T.G., Marhavý, P., and Geldner, N. (2018). A protocol for combining fluorescent proteins with histological stains for diverse cell wall components. Plant J. *93*, 399–412.
40. Llavata-Peris, C., Lokerse, A., Möller, B., De Rybel, B., and Weijers, D. (2013). Imaging of phenotypes, gene expression, and protein localization during embryonic root formation in Arabidopsis. Methods Mol. Biol. *959*, 137–148.
41. Lin, K., Kools, H., de Groot, P.J., Gavai, A.K., Basnet, R.K., Cheng, F., Wu, J., Wang, X., Lommen, A., Hooiveld, G.J., et al. (2011). MADMAX - Management

and analysis database for multiple ~omics experiments. J. Integr. Bioinform. *8*, 160.

42. Bolstad, B.M., Irizarry, R.A., Astrand, M., and Speed, T.P. (2003). A comparison of normalization methods for high density oligonucleotide array data based on variance and bias. Bioinformatics *19*, 185–193.
43. Irizarry, R.A., Bolstad, B.M., Collin, F., Cope, L.M., Hobbs, B., and Speed, T.P. (2003). Summaries of Affymetrix GeneChip probe level data. Nucleic Acids Res. *31*, e15.
44. Dai, M., Wang, P., Boyd, A.D., Kostov, G., Athey, B., Jones, E.G., Bunney, W.E., Myers, R.M., Speed, T.P., Akil, H., et al. (2005). Evolving gene/transcript definitions significantly alter the interpretation of GeneChip data. Nucleic Acids Res. *33*, e175.
45. Shannon, P., Markiel, A., Ozier, O., Baliga, N.S., Wang, J.T., Ramage, D., Amin, N., Schwikowski, B., and Ideker, T. (2003). Cytoscape: a software environment for integrated models of biomolecular interaction networks. Genome Res. *13*, 2498–2504.

STAR★METHODS

KEY RESOURCES TABLE

REAGENT or RESOURCE	SOURCE	IDENTIFIER
Bacterial and Virus Strains		
Agrobacterium tumefaciens C58 PMP90	N/A	N/A
Escherichia coli DH5α	Thermo-Fisher	Cat# 18265017
Chemicals, Peptides, and Recombinant Proteins		
5-bromo-4-chloro-3-indolyl β-D-glucopyranoside-sodium salt(X-Glc)	X-Gluc Direct	N/A
6-Benzylaminopurine	Duchefa Biochemie	Cat# B0904
ATP	New England Biolabs	Cat# P0765
BbsI	New England Biolabs	Cat# R3539
BsaI	New England Biolabs	Cat# R0535
Calcofluor White	Sigma-Aldrich	Cat# 18909
Carbenicillin	Duchefa Biochemie	Cat# C0109
Dexamethasone	Sigma-Aldrich	Cat# D4902
Dimethyl sulfoxide	Sigma-Aldrich	Cat# 472301
Dimethylformamide (DMF)	Sigma-Aldrich	Cat# D4092
Glycerol	Sigma-Aldrich	Cat# G6279
Kanamycin	Duchefa Biochemie	Cat# K0126
Lactic acid	Arcos Organics	Cat# 189870010
MES	Duchefa Biochemie	Cat# M01503
MS-salt	Duchefa Biochemie	Cat# M0221
Paraformaldehyde	Sigma-Aldrich	Cat# 158127
Potassium Ferricyanide (K3Fe(CN)6)	Sigma-Aldrich	Cat# 702587
Potassium Ferrocyanide (K4Fe(CN)6)	Sigma-Aldrich	Cat# P9837
Propidium Iodide	Sigma-Aldrich	Cat# P4170
Q5 High-Fidelity DNA polymerase	New England Biolabs	Cat# M0491
Rifampicin	Duchefa Biochemie	Cat# R0146
SCRI Renaissance Stain 2200	Renaissance Chemicals	N/A
Silwet	Lehle Seeds	Cat# VIS-30
Sodium deoxycholate	Sigma-Aldrich	Cat# 30970
Sodium metabisulphite	Merck	Cat# 106528
Spectinomycin	Duchefa Biochemie	Cat# S0188
T4-DNA Ligase	New England Biolabs	Cat# M0202
Triton X-100	Merck	Cat# 11869
Urea	USB	Cat# 75826
Xylitol	Sigma-Aldrich	Cat# X3375
Critical Commercial Assays		
GeneJET Plasmid Miniprep Kit	Thermo-Fisher	Cat# K0503
iScript cDNASynthesis Kit	Bio-Rad	Cat# 1708890
LightCycler 480 SYBR Green I Master	Roche Diagnositics	Cat# 50-720-3180
MultiSite Gateway™ Pro Plus	Thermo-Fisher	Cat# 12537100
NEB Golden Gate Assembly Kit	New England Biolabs	Cat# E1601
RNeasy Plus Mini Kit	QIAGEN	Cat# 74136
Deposited Data		
Transcriptomics datafiles	Gene Expression Omnibus	GEO: GSE116858

(*Continued on next page*)

Continued

REAGENT or RESOURCE	SOURCE	IDENTIFIER
Experimental Models: Organisms/Strains		
Arabidopsis: Col-0	Nottingham *Arabidopsis* Stock Centre	N/A
Arabidopsis: *dof2.1-1*	MPI for Plant Breeding Research; Cologne, Germany [27]	GK-668G12
Arabidopsis: *dof2.1-2*	This paper	N/A
Arabidopsis: *dof2.1-2 tmo6-1 dof6-2*	This paper	N/A
Arabidopsis: *lhw*	[4]	N/A
Arabidopsis: p*DOF2.1*::DOF2.1:sYFP	This paper	N/A
Arabidopsis: p*DOF2.1*::GFP/GUS	This paper	N/A
Arabidopsis: p*DOF6*::erVENUS	This paper	N/A
Arabidopsis: p*LOG4*::tdTomato	This paper	N/A
Arabidopsis: p*RPS5A*::DOF2.1	This paper	N/A
Arabidopsis: p*RPS5A*::DOF2.1-GR	This paper	N/A
Arabidopsis: p*RPS5A*::LHW:GR	This paper	N/A
Arabidopsis: p*RPS5A*::nGFP-GUS	This paper	N/A
Arabidopsis: p*RPS5A*::TMO5:GR	[4]	N/A
Arabidopsis: p*RPS5A*::TMO5:GR x p*RPS5A*::LHW:GR	This paper	N/A
Arabidopsis: pTCSn::ntdTomato - pDR5revV2::n3GFP	This paper	N/A
Arabidopsis: p*TMO6*::erRFP	This paper	N/A
Arabidopsis: *tmo5 tmo5-like1*	[4]	N/A
Arabidopsis: *tmo6-1 dof6-2*	This paper	N/A
Arabidopsis: *tmo6-4 dof6-1*	This paper	N/A
Arabidopsis: *wol*	[28]	N/A
Arabidopsis: *dof6-1*	Nottingham *Arabidopsis* Stock Centre	WiscsDsLox351c08
Oligonucleotides		
See table S1	N/A	N/A
Recombinant DNA		
pBGWFS7	VIB-Ugent Center For Plant Systems Biology	https://gateway.psb.ugent.be/
pBGWFS7 p*DOF2.1*::GFP/GUS	This paper	N/A
p*DOF2.1*::DOF2.1:sYFP	This paper	N/A
pDONR221	Thermo-Fisher	N/A
pDONRP2RP3	Thermo-Fisher	N/A
pDONRP4P1R	Thermo-Fisher	N/A
pDONRP4-P1R *pRPS5A*	This paper	N/A
pFASTRK_AtCas9_AG	[29]	N/A
pGG-A-ATU6PTA-B	[29]	N/A
pGG-B-ATU6PTA-C	[29]	N/A
pGG-C-ATU6PTA-D	[29]	N/A
pGG-D-ATU6PTA-E	[29]	N/A
pGG-D-ATU6PTA-E	[29]	N/A
pGIIM/LIC_SwaI-ntdTomato - pDR5revV2-n3GFP	[30]	N/A
pHm34GW	VIB- UGent Center For Plant Systems Biology	https://gateway.psb.ugent.be/
pHm34GW p*DOF6*::erVENUS	This paper	N/A
pHm34GW p*TMO6*::erRFP	This paper	N/A

(*Continued on next page*)

Continued		
REAGENT or RESOURCE	SOURCE	IDENTIFIER
pHm42GW	VIB-UGent Center For Plant Systems Biology	https://gateway.psb.ugent.be/
pHm42GW p*RPS5A*::DOF2.1	This paper	N/A
pHm43GW	VIB-UGENT Center For Plant Systems Biology	https://gateway.psb.ugent.be/
pHm43GW p*RPS5A*::DOF2.1-GR	This paper	N/A
pMK7S-NFm14GW,0 p*RPS5A*	VIB- UGent Center For Plant Systems Biology	https://gateway.psb.ugent.be/
p*RPS5A*::LHW:GR	This paper	N/A
p*RPS5A*::nGFP-GUS	This paper	N/A
pTCSn::ntdTomato	[31]	N/A
pTCSn::ntdTomato - pDR5revV2::n3GFP	This paper	N/A
Software and Algorithms		
BoxPlotR	N/A	http://shiny.chemgrid.org/boxplotr/; RRID:SCR_015629
CRISPR-P	[32]	http://crispr.hzau.edu.cn/CRISPR/
Cytoscape	N/A	https://cytoscape.org; RRID:SCR_003032
Microsoft Excel	Microsoft	RRID:SCR_016137
GENIST	[15]	https://github.com/madeluis/GENIST/commits/master
ImageJ	N/A	https://imagej.nih.gov/ij/; RRID:SCR_003070
Leica Application Suite X	Leica Microsystems	https://www.leica-microsystems.com; RRID:SCR_013673
qBASE+	Biogazelle	https://www.qbaseplus.com/; RRID:SCR_003370
Other		
Leica SP2 confocal microscope	Leica Microsystems	N/A
Leica SP8 confocal microscope	Leica Microsystems	N/A
LightCycler 480	Roche Life Sciences	N/A
Olympus BX53	Olympus Lifesciences	N/A

CONTACT FOR REAGENT AND RESOURCE SHARING

Further information and requests for resources and reagents should be directed to and will be fulfilled by Bert De Rybel (beryb@psb.vib-ugent.be).

EXPERIMENTAL MODEL AND SUBJECT DETAILS

Arabidopsis thaliana (L.) Heynh. background lines Columbia-0 (Col-0), were used for experimentation, with mutants and transgenic lines in these backgrounds as detailed in the Key Resources Table. *Arabidopsis* seedlings were cultivated at 22°C under continuous light conditions.

METHOD DETAILS

Plant material and growth conditions

All seeds were surface sterilized, sown on solid ½ MS plates without sucrose, and stratified for 24h at 4°C two days before they were grown at 22°C in continuous light conditions. Ten day old seedlings were transferred to soil and grown in green house conditions. Dexamethasone (DEX) treatment was performed by either germinating seeds on 10μM DEX-supplemented medium or by transferring plants from ½ MS to 10μM DEX supplemented medium and continuing growth for the indicated time. Benzyl Adenine (BA) treatment

was performed by transferring plants from ½ MS to 10μM BA supplemented medium and continuing growth for the indicated time. Both BA and DEX were dissolved in dimethyl sulfoxide. The *dof2.1-1* T-DNA mutant used (GK-668G12) was generated in the context of the GABI-Kat program and provided by Bernd Weisshaar (MPI for Plant Breeding Research; Cologne, Germany) [27]. The *Arabidopsis thaliana* (L.) Heynh. Col-0 ecotype served as wild-type control in all experiments. The AGI identifiers for the genes used in this study were as follows: *DOF2.1*: *AT2G28510*, *TMO6*: *AT5G60200*, *DOF6*: *AT3G45610*, *TMO5*: *AT3G25710*, *LHW*: *AT2G27230*, *LOG3*: *AT2G37210*, *LOG4*: *AT3G53450*, *ARR1*: *AT3G16857*, *ARR10*: *AT4G31920*, *ARR12*: *AT2G25180*, *SACL3*: *AT1G29950*, *ACL5*: *AT5G19530*.

Cloning and plant transformation

The p*RPS5A*::*TMO5*:GR x p*RPS5A*::*LHW*:GR or dGR line was generated by first fusing the LHW coding sequence to the mammalian glucocorticoid receptor (GR) and driving this from the strong meristematic *RPS5A* promoter [10] using LIC cloning [33, 34]. This p*RPS5A*::LHW:GR line was next crossed into the existing p*RPS5A*::TMO5:GR line [4] to obtain the dGR line. The pTCSn::ntdTomato - pDR5revV2::n3GFP [30, 31] construct was generated by using PCR to generate the TCSn promoter fragment with appropriate LIC adapters. This was inserted into the pGIIM/LIC_SwaI-ntdTomato - pDR5revV2-n3GFP destination vector [30] using the LIC cloning system. Other vectors were generated using Gateway Technology (Thermo-Fisher). p*RPS5A*::DOF2.1 was generated by cloning the DOF2.1 genomic sequence in the pDONR221 entry vector and subsequently recombining it with the p*RPS5A* pDONRP4P1R in the pHm42GW destination vector. p*RPS5A*::DOF2.1-GR was generated by cloning DOF2.1 genomic sequence without stop in the pDONR221 entry vector and subsequently recombining it with the p*RPS5A* pDONRP4P1R and GR pDONRP2RP3 in a pHm43GW destination vector. The DOF2.1 promoter was obtained by amplifying the 3711bp upstream region of the transcriptional start and cloning this into the pDONRP41R entry vector. p*DOF2.1*::GFP/GUS was generated by cloning the *DOF2.1* promoter region in pBGWFS7 destination vector using Gateway cloning. The TMO6 and DOF transcriptional fusions were generated by cloning the promoter regions into the pDONRP41R entry vector and combining these with erRFP and erVENUS respectively into the pHm34GW destination vector. p*DOF2.1*::DOF2.1:sYFP was obtained by cloning the p*DOF2.1*, DOF2.1 genomic sequence minus stop, and sYFP entry clones in the pHm43GW destination vector using Gateway cloning. p*RPS5A*::nGFP-GUS was generated by amplifying the p*RPS5A* promoter sequence [10] and cloning this into the pDONRP4P1R and subsequently cloning this into the pMK7S-NFm14GW,0 destination vector. All constructs were verified by Sanger sequencing and were transformed into Col-0 using simplified floral dipping. All primer sequences used for cloning and sequencing can be found in Data S1.

CRISPR/CAS9 mutant generation

Two guide RNAs (gRNAs) were designed per gene using the CRISPR-P tool [32]. Cloning of gRNA vectors was performed essentially as previously described [29]. Briefly, gRNA oligos were appended with the corresponding overlaps (FW: 5′-ATTG REV: 5′-AAAC) to enable annealed-oligo cloning. Primers used for cloning and sequencing can be found in Data S1. Oligos were annealed and ligated into six Golden Gate gRNA entry modules using standard DNA ligation and sequenced verified. The gRNA entry plasmids were cloned into the pFASTRK_AtCas9_AG destination vector (https://gateway.psb.ugent.be) using Golden Gate assembly. Expression vectors were sequenced to verify successful insertion of the gRNAs. Positive expression vectors were transformed into *Agrobacterium tumefaciens* C58 PMP90. Plants were transformed with Agrobacterium cultures using floral dip. Transformed events were selected based on red seed fluorescence and sown on soil. Knockout mutations in the target genes were confirmed in the T1 generation by PCR amplification and Sanger sequencing followed by TIDE analysis [35]. T2 seeds lacking red seed fluorescence (Cas9 null segregants) were sown on soil and plants again screened for the desired editing events. Cas9-free, homozygous knockout plants were selected and seeds harvested. Desired editing events were confirmed in T3 generation by Sanger sequencing. T3 seeds were used for all experiments.

Plant imaging and image processing

For differential interference contract (DIC) microscopy, samples were mounted in a solution of 20% glycerol 60% lactic acid and imaged using an Olympus BX53 microscope equipped with DIC optics. Expression of pDOF2.1::GFP-GUS for DIC analysis was visualized using GUS staining as described in [36].Cell wall staining for optical cross sections was done using modified Pseudo Schiff – Propidium Iodine (mPS-PI) [37]. Marker lines were cleared using the ClearSee protocol [38] including a cell wall staining with 0.1% Calcofluor White [39]. Confocal microscopy was performed on Leica SP8 (40X) and Leica SP2 (63X) (all water corrected objective lenses with NA 1.2) confocal microscopes. Calcofluor White, GFP, sYFP, tandemTomato (tdT) and propidium iodide (PI) samples were imaged at an excitation of 405nm, 488nm, 514nm, 561nm and 514nm respectively. Calcofluor White, GFP, tdT and PI were visualized at an emission of 425-475 nm, 500-535nm, 520-550nm, 580-630nm and 600-700nm respectively. Embryos were fixed and stained using Renaissance [40]. Embryos were popped out of the ovules and R2200 and GFP were visualized by excitation at 405 and 488 nm and detection between 430-470 nm and 500-535 nm, respectively

qRT-PCR

RNA was extracted with the RNeasy kit (QIAGEN). Poly(dT) cDNA was prepared from 1 mg of total RNA with an iScript cDNA Synthesis Kit (Bio-Rad) and analyzed on a LightCycler480 apparatus (Roche) with SYBR GREEN I Master kit (Roche) according to

the manufacturer's instructions. Primer pairs were designed with the Universal Probe Library Assay Design Center (Roche). Experiments were repeated in triplicate, each with three technical replicates. Data was analyzed using qBase+ software package (Biogazelle). Expression levels were normalized to those of EEF1α4 and CDKA1;1. All primers used for qRT-PCR analysis can be found in Data S1

Whole genome transcriptome analysis

pRPS5A::TMO5:GR x pRPS5A::LHW:GR (dGR) and Col-0 seeds were bleach sterilized and stratified for 24h at 4°C. Seeds were sown on ½ MS plates and grown for 5 days in a growth room at 22°C. 5-day old plants of both Col-0 and dGR were transferred to ½ MS plates containing 10 μM DEX and mock-plates and were sampled at the following time points: 0h, 0.5h, 1h, 2h, 3h, 4h, 5h and 6h. 300 individual root tips were sampled per sample and three biological repeats per time point were used. Root tips were harvested directly into liquid nitrogen, RNA was extracted using the RNeasy kit (QIAGEN). Total RNA (100 ng) was labeled using an Ambion WT expression kit (Life Technologies) and hybridized to *Arabidopsis* Gene 1.0 ST arrays (Affymetrix), that probes the expression of 27,827 unique genes. Sample labeling; hybridization to chips and image scanning was performed according manufacturer's instructions. Microarray analysis was performed using MADMAX pipeline for statistical analysis of microarray data [41]. Expression values were calculated using robust multichip average (RMA) method, which includes quantile normalization [42, 43]. Probe sets on the array were redefined using current genome information [44]. In this study, probes were reorganized on the basis of the gene definitions as available in the TAIR10 database.

Network inference

To infer a gene regulatory network (GRN) and predict the causal relationships of genes regulated by TMO5 and LHW, differentially expressed genes (DEGs) were identified using $q < 0.05$ & fold change > 2 as our selection criteria, when performing pairwise comparisons between hours 0-0.5, 0-1, 0-2, 0-3, 0-4, 0-5, and 0-6 of the TMO5/LHW induction time course. This resulted in the identification of 237 genes differentially expressed at 0.5, 1, 2, 3, 4, 5, and 6 hours after TMO5/LHW induction, which contained 22 transcription factors (Table S2). To preserve the temporal cascade of regulations, the network was inferred as individual GRNs containing the DEGs at each time point, as opposed to predicting a GRN containing the 237 DEGs together. Specifically, because we assume that regulation between genes can occur, not only during concurrent time points, but also between consecutive time points, the DEGs from consecutive time points were grouped (0.5-1, 1-2, 2-3, 3-4, 4-5, 5-6 hours), and GRNs from each of the 6 resulting lists of genes were inferred. The GRN inference on each of the 6 sets of DEGs was performed by applying a dynamic Bayesian network (DBN)-based inference algorithm, GENIST [15]. Since GENIST offers the possibility of clustering genes based on their co-expression prior the inference step to improve the performance of the algorithm, GENIST was ran using a previously published TMO5-GR dataset (TMO5 induced for short time points and a cell sorted set) [3] for the clustering step. Details about the application of GENIST to each of the 6 sets of genes are provided below.

1. Gene selection

The genes differentially expressed at each time point after induction of TMO5/LHW, g_t, for $t \in \{0.5,\ 1,\ 2,\ 3,\ 4,\ 5,\ 6\}$ hours were selected. Then, the DEG from every two consecutive time points, g_t and g_{t+1}, were combined in sets $S\tau$, *for* $\tau \in \{0.5\&1, 1\&2,\ 2\&3,\ 3\&4,\ 4\&5,\ 5\&6\}$. Steps 2 and 3 were applied to the genes in each set S_ϕ individually.

2. Clustering

The expression values from the TMO5 induction from De Rybel et al., 2014 were used as the input data. Clustering of the genes in S_ϕ was implemented by using the Silhouette index followed by linkage clustering. This resulted in a division of the $S_\phi$genes in c clusters.

3. GRN inference

3.1. Inferring intra-cluster connections for each cluster C_n, *for* $n \in [1, c]$*:* The expression values in the TMO5/LHW induction time course for all genes in cluster C_n were used as the input data.

3.1.1 Selecting potential regulators: A gene g_r was selected as a potential regulator of a target gene g_s (denoted $g_r \rightarrow g_s$) if it exhibited a $\pm p \times g_r$ change of expression immediately prior a change of expression of $g_s$of $\pm p \times g_s$:

$$g_r \rightarrow g_s \leftrightarrow (g_r(t) > (1+p) \times g_r(t-1) | g_r(t) < (1-p) \times g_r(t-1)) \ \&\ (g_s(t+1) > (1+p) \times g_s(t) | g_s(t+1) < (1-p) \times g_s(t)) \quad (1)$$

where we set a low threshold $(p = 0.1)$ to ensure that no regulators were missed.

3.1.2. DBN modeling: The GRN inference step was implemented as a Dynamic Bayesian Network (DBN) learning problem, where the dependences among the variables (genes) can be derived over adjacent time steps. Assuming stationarity and the genes to be modeled obeyed the first order Markov assumption, the joint probability distribution could be expressed as:

$$P(X_1, \ldots, X_m) = \prod_i P(X_i | X_1, \ldots, X_{i-1}) = \prod_i P(X_i | Pa(X_i)) \quad (2)$$

where X_i is the expression of gene i, $m = n(T-1)$ is the number of genes (nodes), and $Pa(X_i)$ is the set of regulators of gene i (parents of node i).

Given some observations of the variables over time, the DBN estimation was implemented by finding the structure of (2) that maximized the Bayesian Dirichlet equivalence uniform (BDeu) score [3]. Since the BDeu score of a DBN can be decomposed as the sum of the scores of the log conditional probabilities of each node, the log of the BDeu, BDeul, was used:

$$BDeu_l(D,G) = \log(P(G)) + \sum_{i=1}^{n}\sum_{j=1}^{q_i}\left(\log\left(\frac{\Gamma\left(\frac{б}{q_i}\right)}{\Gamma\left(\sum_{k=1}^{r_i} N_{ijk} + \frac{б}{q_i}\right)}\right)\right) + \sum_{k=1}^{r_i}\log\left(\frac{\Gamma\left(N_{ijk} + \frac{б}{q_i}\right)}{\Gamma\left(\frac{б}{r_i q_i}\right)}\right) \quad (3)$$

where G refers to the Bayesian graph, D refers to the dataset containing the observations of the system, N_{ijk} indicates the number of data vectors in which gene i,X_i, has the value k while its parents are in the jth configuration, and б refers to the hyperparameters of the Dirichlet distribution.

From (2) and (3), the problem of deriving the DBN can be decomposed into finding the parents for each node. For this, the expression values of each gene were discretized in 2 levels (high and low). Then, for each gene, a list of all possible subsets of potential regulators was generated. To lower the complexity of the algorithm, which increases exponentially with the number of genes, the maximum size allowed for any subset (maximum number of regulators of a gene) was set to 3. The $BDeu_l$ was used to evaluate the likelihood that each gene was due to each subset of potential regulators. The regulators of gene i were selected as the ones contained in the subset that led to the highest value of the $BDeu_l$.

3.2. Inferring inter-cluster connections: Steps 3.1.1-3.1.2 were repeated for all hubs (cluster node with the largest degree of edges leaving the node (out-degree)) in all clusters Cn, for $n \in [1,c]$. This resulted in inter-cluster interactions among the cluster hubs.

3.3. Determining the sign of the interactions: A score was implemented to estimate whether the inferred interactions (edges) were activations or repressions. The score was calculated for each edge as the conditional probability that a gene is expressed (or not expressed) given that a parent was expressed (not expressed) in the prior time point, relative to the probability that a gene is expressed (or not expressed) given that a parent was not expressed (or vice versa expressed) in the prior time point. If the first conditional probability is larger (or smaller) than the second one, then the parent was found to be an activator (or repressor). In the case of a tight, the edge was found to have an undetermined sign.

The application of GENIST with this data resulted in 6 networks, corresponding to the 6 sets of DEGs, $S_ф$. To illustrate the cascade of regulations through time, the networks for each set were jointly visualized in Cytoscape [45]. The final network has 237 nodes, corresponding to the 237 DEGs, and 532 edges (regulations). The thickness each edge correlates with the probability with which the corresponding regulation was calculated (as in (3)), and the size of each node correlates with the number of genes that it directly regulates. The predicted most important regulators can be identified as the largest nodes in the network. The network depicts the time cascade by color-coding the regulations inferred in the different time points: red (0.5-1), green (1-2), blue (2-3), yellow (3-4), pink (4-5), orange (5-6) hours. Overall, the network places the initial time points at the center, and shows how the cascade of regulations expands outward over time.

QUANTIFICATION AND STATISTICAL ANALYSIS

All violin plots were generated using the BoxPlotR webtool using standard settings (http://shiny.chemgrid.org/boxplotr). In all plots, center lines represent the medians; box limits indicate the 25th and 75th percentiles as determined by R software; whiskers extend 1.5 times the interquartile range from the 25th and 75th percentiles, outliers are represented by dots. The number of samples analyzed is indicated on the top of the x axis for each sample when relevant. In the quantification of IPC cell number, one single outlier was removed before statistical analysis. Pairwise comparisons were performed using standard two-sided Student t testing. In all cases, * indicates a p value < 0.05 and ** indicates a p value < 0.001. In case of multiple samples, a one-way ANOVA analysis with post hoc Tukey HSD testing was performed. Significantly different groups (p value < 0.001) of samples are indicated using lower case letters.

DATA AND SOFTWARE AVAILABILITY

The transcriptomics data files are deposited on the Gene Expression Omnibus (accession number GEO: GSE116858).